Excited-state quantum phase transitions in the interacting boson model: Spectral characteristics of 0^{+} states and effective order parameter

Yu Zhang, Yan Zuo, Feng Pan, and J. P. Draayer

Phys. Rev. C **93**, 044302 — Published 4 April 2016

DOI: 10.1103/PhysRevC.93.044302

Excited-state quantum phase transitions in the interacting boson model: spectral characteristics of 0^+ states and the effective order parameter

Yu Zhang,[1] Yan Zuo,[1] Feng Pan,[1,2] and J. P. Draayer[2]

[1]*Department of Physics, Liaoning Normal University, Dalian 116029, P. R. China*
[2]*Department of Physics and Astronomy, Louisiana State University, Baton Rouge, LA 70803-4001, USA*

(Dated: March 21, 2016)

The spectral characteristics of the $L^\pi = 0^+$ excited-states in the interacting boson model are systematically investigated. It is found that various types of excited-state quantum phase transitions may widely occur in the model as functions of the excitation energy, which indicates that the phase diagram of the interacting boson model can be dynamically extended along the direction of the excitation energy. It has also been justified that the d-boson occupation probability $\rho(E)$ is qualified to be taken as the effective order parameter to identify these excited-state quantum phase transitions. In addition, the underlying relation between the excite-state quantum phase transition and the chaotic dynamics is also stated.

PACS numbers: 21.60.Fw, 03.65.Fd, 64.60.-i

I. INTRODUCTION

Quantum phase transition (QPT) is an interesting and important subject for many subfields. The quantum phase transition is not of the usual thermodynamic type, but related to changes in the shape of the ground state at zero temperature, which is thus also called the shape phase transition or ground-state QPT (GSQPT). In theory, algebraic approaches provide convenient ways to investigate the QPTs in mesoscopic systems. The best examples may be the interacting boson model (IBM) [1] for nuclear structure and the vibron model (VM) [2] for molecules and atomic clusters. Recent reviews on the GSQPTs in nuclei are given in [3–5].

More recently, considerable attention has been given to the so-called excited-state quantum phase transition (ESQPT) [6–19]. Unlike GSQPT, an ESQPT can occur not only with variation of the control parameters of a model Hamiltonian, but also with the increasing of the excitation energy. In short, ESQPTs may occur in excited states [14]. Most of the studies of ESQPTs currently focus on the theoretical side and were carried in two-level boson or fermion models with pairing interactions [14]. Typical examples are the U(5)-SO(6) ESQPT [9–11] in the IBM and the U(2)-SO(3) ESQPT [15, 16] in the two dimensional limit of the VM. ESQPTs in other many-body quantum systems have also been investigated, such as those in the Lipkin-Meshkov-Glick (LMG) model [20, 21], the Jaynes-Cummings model [22, 23], the Dicke model [22–24], and the kicked-top model [25]. Generally, ESQPTs emerge in the systems with a large number of particles. A basic feature of the ESQPT, such as the U(5)-SO(6) ESQPT, is that there exists a separatrix, which divides the excited states into two sets [16]. Some effective order parameters may show sudden changes around the separatrix [16]. In addition, the separatrix in spectra may extend from the ground state energy to much higher excitation energy. It seems that the GSQPT can propagate from the ground state to excited states [9], which thus indicates a deep relation between the GSQPT and ESQPT.

The IBM [1] provides an ideal theoretical framework to investigate the GSQPTs in different transitional regions [4].

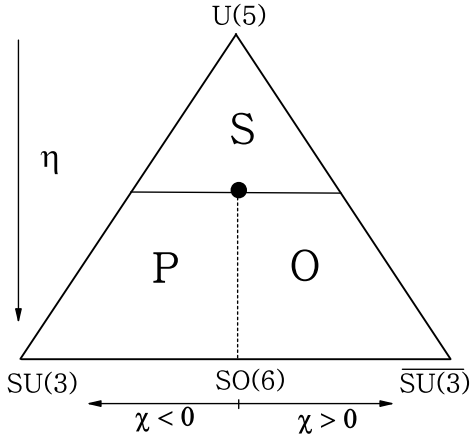

FIG. 1: (Color online) Phase diagram in the IBM parameter space, where S represents the region with $\beta_e = 0$ corresponding to the spherical, P represents the region with $\beta_e > 0$ corresponding to the prolate, and O represents the region with $\beta_e < 0$ corresponding to the oblate. In addition, the dashed lines denote the critical points of the first-order QPTs, while the solid dot in the center represents the triple point.

There may exist three typical GSQPTs in the IBM if only up to two-body interactions are taken into consideration, namely the U(5)-SO(6) GSQPT, the U(5)-SU(3) GSQPT, and the SU(3)-$\overline{\text{SU(3)}}$ GSQPT. These GSQPTs have been widely discussed both in the theory and in experiment. But only the U(5)-SO(6) ESQPT was previously emphasized in the IBM [9–11, 14]. In this work, we make a systematic analysis of the spectral evolutions in different transitional regions to figure out whether or not the main features appearing in the U(5)-SO(6) ESQPT [14] also emerge in other transitional regions of the IBM. It should be mentioned that all numerical calculations are carried out by using the IBAR code [26], which makes a large-N calculation in the IBM possible.

II. THE MODEL HAMILTONIAN AND THE ASSOCIATED GSQPTS

A Hamiltonian in the IBM framework is constructed from two kinds of boson operators; s-boson with $J^\pi = 0^+$ and d-boson with $J^\pi = 2^+$ [1]. Specifically, we consider the IBM consistent-Q Hamiltonian [27]

$$\hat{H}(\eta,\,\chi) = \varepsilon\left[(1-\eta)\hat{n}_d - \frac{\eta}{4N}\hat{Q}^\chi\cdot\hat{Q}^\chi\right], \qquad (1)$$

where $\hat{Q}^\chi = (d^\dagger s + s^\dagger\tilde{d})^{(2)} + \chi(d^\dagger\tilde{d})^{(2)}$ is the quadrupole operator, η and χ are the control parameters with $\eta\in[0,1]$ and $\chi\in[-\sqrt{7}/2,\sqrt{7}/2]$, and ε is a scale factor, which will be set as 1 for convenience. It can be proven that the Hamiltonian is in the U(5) DS when $\eta = 0$; it is in the O(6) DS when $\eta = 1$ and $\chi = 0$; it is in the SU(3) DS when $\eta = 1$ and $\chi = -\frac{\sqrt{7}}{2}$; it is in the $\overline{\mathrm{SU(3)}}$ DS when $\eta = 1$ and $\chi = \frac{\sqrt{7}}{2}$. To identify the GSQPTs in the IBM, one may calculate the expectation value of the Hamiltonian (1) in the coherent state defined as [1]

$$\begin{aligned}|\beta,\gamma,N\rangle &= \frac{1}{\sqrt{N!(1+\beta^2)^N}}[s^\dagger + \beta\cos\gamma\, d_0^\dagger \\ &+ \frac{1}{\sqrt{2}}\beta\sin\gamma(d_2^\dagger + d_{-2}^\dagger)]^N|0\rangle\,, \qquad (2)\end{aligned}$$

which provides the scaled potential surface in the large-N limit with

$$\begin{aligned}V_{\rm s}(\beta,\gamma) &= \frac{1}{N}\langle\beta,\gamma,N|H|\beta,\gamma,N\rangle|_{N\to\infty} \\ &= (1-\eta)\frac{\beta^2}{1+\beta^2} - \frac{\eta}{4(1+\beta^2)^2} \\ &\times [4\beta^2 - 4\sqrt{\frac{2}{7}}\chi\beta^3\cos3\gamma + \frac{2}{7}\chi^2\beta^4]\,. \qquad (3)\end{aligned}$$

To illustrate types and orders of the QPTs, one should minimize the potential function (3) by varying β and γ for given η and χ. The optimal values are denoted as $\beta_{\rm e}$ and $\gamma_{\rm e}$, with which one can get the ground state energy per boson defined as $E_g = V_s(\eta,\chi,\beta_{\rm e},\gamma_{\rm e})$. It can be found that the γ-dependence in (3) yields either $\gamma_{\rm e} = 0^\circ$ or $\gamma_{\rm e} = 60^\circ$, but the case of $\gamma_{\rm e} = 60^\circ$ can be equivalently described by substituting $\gamma_{\rm e} = 0^\circ$ and $\beta_e = -\beta_{\rm e}$. We henceforth set $\gamma = 0^\circ$ in the following for convenience, and only study its β-dependence. Here, $\beta_{\rm e} = 0$, $\beta_{\rm e} > 0$, and $\beta_{\rm e} < 0$ represent the spherical, prolate, and oblate deformations, respectively. β_e can thus serve as the order parameter to be used to identify the different shape phases and the associated GSQPTs [28]. On the other hand, one can also identify the GSQPTs and their orders from the ground state energy E_g. For the second-order QPT, E_g and $\frac{\partial E_g}{\partial x}$ are continuous, but $\frac{\partial^2 E_g}{\partial x^2}$ is not, where x represents the corresponding control parameter. For the first-order QPT, it requires that E_g is continuous, but $\frac{\partial E_g}{\partial x}$ is not [28]. Based on these criteria, one can prove that the system may experience the first-order QPTs in two directions with variation of the control parameters η and χ [29]. Specifically, the critical point of the first-order QPTs occurring along the η direction are given as

$$\eta_c = \frac{14}{28+\chi^2} \qquad (4)$$

with $\chi\in[-\sqrt{7}/2,\sqrt{7}/2]$ and those along the χ direction are given as $\chi_c = 0$ with $\eta\in(0.5,1]$. In addition, the U(5)-SO(6) GSQPT occurring at the critical point $\eta_c = 0.5$ (also called the triple point [29]) is the unique second-order transition [1] in the IBM described by (1). The two-dimensional parameter space of the IBM described by (1) can be mapped onto a symmetric triangle [29] called the extended Casten triangle as shown in Fig. 1, which may cover all types of GSQPTs in the IBM described by a Hamiltonian with up to two-body terms.

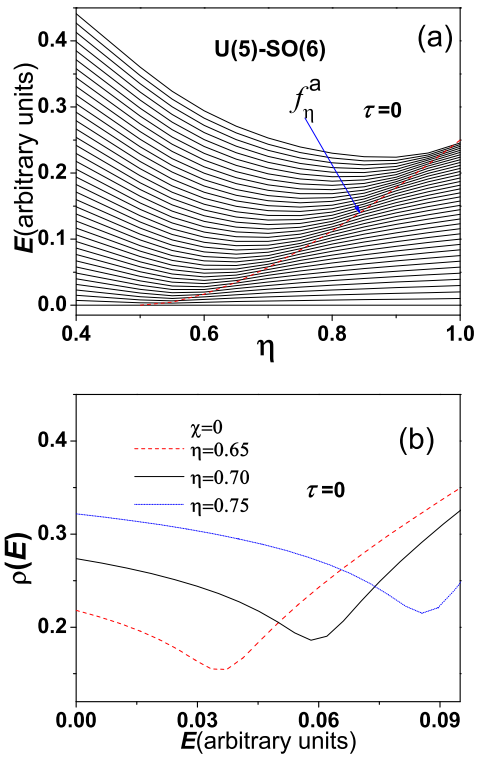

FIG. 2: (Color online) (a) The excitation-energy spectrum of the lowest 40 $\tau = 0$ levels obtained from the U(5)-SO(6) Hamiltonian (1) with $\chi = 0$ and $N = 100$. (b) The effective order parameter ρ defined in (5) as a function of the excitation energy for three typical η values.

In the following, we will focus on the potential ESQPTs appearing in the U(5)-SO(6), the U(5)-SU(3), and the SU(3)-$\overline{\mathrm{SU(3)}}$ legs, as well as those appearing inside the extended Casten triangle shown in Fig. 1.

III. THE DIFFERENT TYPES OF ESQPTs

A. the U(5)-SO(6) ESQPT

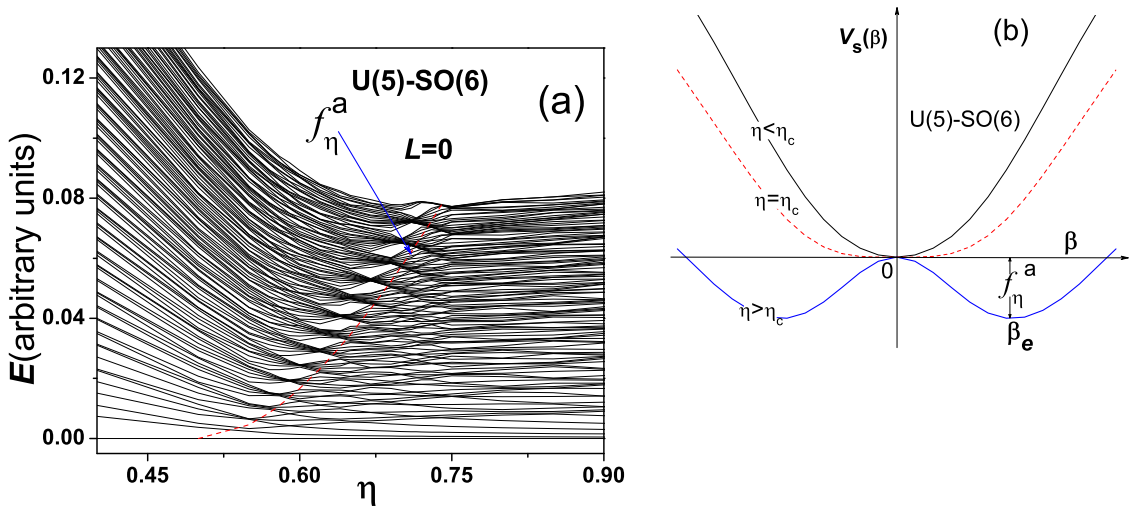

FIG. 3: (Color online) (a) The excitation-energy spectrum of the lowest 124 $L=0$ levels obtained from the U(5)-SO(6) Hamiltonian (1) with $\chi=0$ and $N=100$. (b) The corresponding potential derived from (3) with $\chi=0$, where $\gamma=0^{\circ}$ is always assumed.

As discussed previously, the second-order GSQPT may occur in the U(5)-SO(6) transitional region. Meanwhile, a typical ESQPT has also been identified from the excitation spectrum within the U(5)-SO(6) transitional region [11, 14]. To illustrate the U(5)-SO(6) ESQPT, the first 40 excited levels with $\tau=0$ are obtained from the U(5)-SO(6) Hamiltonian (1) with $\chi=0$ and $N=100$ and the results are shown as functions of the control parameter η in Fig. 2. Here, τ denotes the d-boson seniority number. Hence, $\tau=0$ indicates $L^{\pi}=0^{+}$. To identify the ESQPT, we calculate the d-boson occupation probability for each state, which is defined as

$$\rho=\frac{\langle 0^{+}|\hat{n}_{d}|0^{+}\rangle}{N}, \tag{5}$$

of which the results with $\tau=0$ as functions of the excitation energy for three typical η values are also shown in Fig. 2. This quantity is expected to serve as the effective order parameter [14, 16, 28] to identify the ESQPTs in the IBM. As clearly seen from Fig. 2(a), one can find a separatrix signaling the high density of levels, which form a smooth flow with a "shock wave" propagating from ground state (at the critical point $\eta_c=0.5$) to the top of the spectrum (at $\eta=1$) [9]. More importantly, this separatrix divides the energy levels into two sets: one with the U(5) character (the left-hand side) and the other with the SO(6) character (the right-hand side), which thus indicates an ESQPT from the SO(6)-like dynamics to the U(5)-like dynamics with the increasing of the excitation energy. For convenience, this type of ESQPT is denoted as the U(5)-SO(6) ESQPT since it appears in the U(5)-SO(6) transitional region as shown in Fig. 2. In the large-N limit, the separatrix is defined (see Fig. 3(b)) as the difference between the value of the energy functional (3) with $\chi=0$ evaluated at the local maximum ($\beta=0$) and that at the global minimum ($\beta=\beta_e$) [15, 16]. Specifically, it is given as

$$f_{\eta}^{a}=\begin{cases}0, & 0\leq\eta\leq\eta_c,\\ \frac{4\eta^2-4\eta+1}{4\eta}, & \eta_c<\eta\leq 1.\end{cases} \tag{6}$$

It is clear that the separatrix for $N=100$ can be well described by (6) as shown in panel (a) of Fig. 2. The results in turn indicate that the potential structure in (3) not only reflects the characteristic of the ground state, but also provides the information of the excited states in the IBM even in finite-N cases, which is taken as the basic assumption in the following to define the separatrix functions and the associated spectral patterns in the model. On the other hand, one can find in Fig. 2(b) that the effective order parameter $\rho(E)$ for a given η shows a linear decrement with the increasing of the excitation energy at the beginning and then turns into a linear increment around the separatrix point, which confirms that the ESQPT indeed occurs around the separatrix. Meanwhile, the results also justify that $\rho(E)$ is qualified to be taken as the effective order parameter to identify the U(5)-SO(6) ESQPT [14, 16].

However, the states with $\tau=0$ may often hide in the states with the angular momentum $L=0$ since angular momentum is relatively easier to be identified in a realistic situation. To detect the U(5)-SO(6) ESQPT in the $L=0$ spectrum, the first 124 excited levels with $L=0$ obtained from the same U(5)-SO(6) transitional Hamiltonian are shown in Fig. 3. To emphasize the relation between the U(5)-SO(6) GSQPT and the U(5)-SO(6) ESQPT, the potential evolution in the U(5)-SO(6) transitional region is also shown. As shown in Fig. 3(a), instead of the "shock wave" shown in Fig. 2, a bunching pattern may develop along the line describe by f_{η}^{a}, which is a consequence of the unbroken SO(5) dynamical symmetry of the system according to the analysis given in [9]. It means that the U(5)-SO(6) ESQPT phenomenon remains even in the $L=0$ spectrum. It should be noted that the bunching pattern

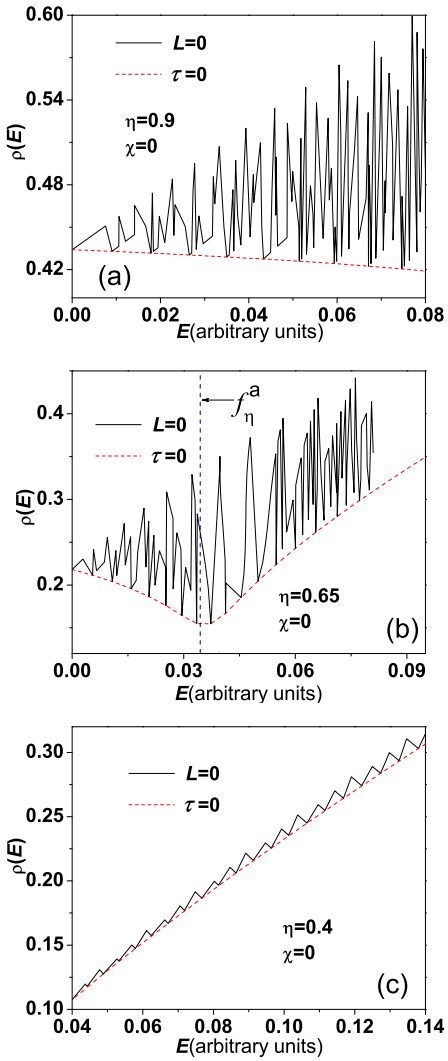

FIG. 4: (Color online) (a) The effective order parameter $\rho(E)$ for $L=0$ obtained from the U(5)-SO(6) Hamiltonian with $N=100$ and $\eta=0.9$ as a function of the excitation energy, where the dashed line denotes the local minima of $\rho(E)$. (b) The same as in (a) but for the results at $\eta=0.65$. (c) The same as in (a) but for the results at $\eta=0.4$.

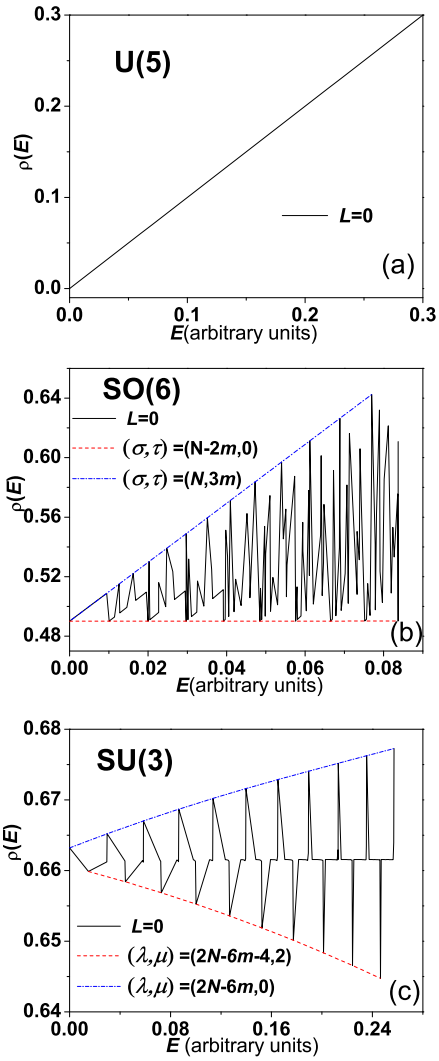

FIG. 5: (Color online) (a) $\rho(E)$ in the U(5) limit for $L=0$ and $N=100$ as a function of the excitation energy. (b) The same as in (a) but for $\rho(E)$ in the SO(6) limit, where (σ,τ) denotes the result corresponding to a given SO(6) irrep with $m=0,\ 1,\ 2....$ (c) The same as in (b) but for $\rho(E)$ in the SU(3) limit, where (λ,μ) represents the results corresponding to a given SU(3) irrep.

constituted by the $L=0$ levels shown in Fig. 3 may appear from $\eta=\eta_c$ to $\eta=1$ if all the 884 $L=0$ levels for $N=100$ are taken into account. In addition, as shown in Fig. 3(b), the ESQPT may appear only when $\eta>\eta_c$ since only the potential with $\eta>\eta_c$ can involve the levels below the separatrix denoted by f_η^a. In the mean-field perspective, the levels below the separatrix should be more heavily affected by the middle hump of the potential with $\eta>\eta_c$ in comparison to those above the separatrix, which may partly answer the origin of the difference in between the SO(6)-like and the U(5)-like spectrum divided by f_η^a in the ESQPT.

To further test the validity of the effective order parameter $\rho(E)$ in the $L=0$ spectrum, the calculated $\rho(E)$ curves as functions of the excitation energy for three typical η values are given in Fig. 4. One can observe in Fig. 4 that the order parameter $\rho(E)$ generally shows a fluctuating behavior as changing of the excitation energy, but the local minima denoted by the dashed line in each case just coincide with those with $\tau=0$, such as those shown in Fig. 2(b). Specifically, the results shown in Fig. 4(a) display a typical behavior of $\rho(E)$ in the SO(6)-like spectrum and those shown in Fig. 4(c) show a typical behavior of $\rho(E)$ in the U(5)-like spectrum. In contrast, the behavior of $\rho(E)$ shown in Fig. 4(b) indicates that an ESQPT may occur around $E=0.04$ when $\eta=0.65$, which is actually consistent with the results shown in Fig. 2(b). It thus confirms that $\rho(E)$ is still qualified to be taken as the effective order parameter to identify the occurrence of the U(5)-SO(6) ESQPT in the $L=0$ spectrum.

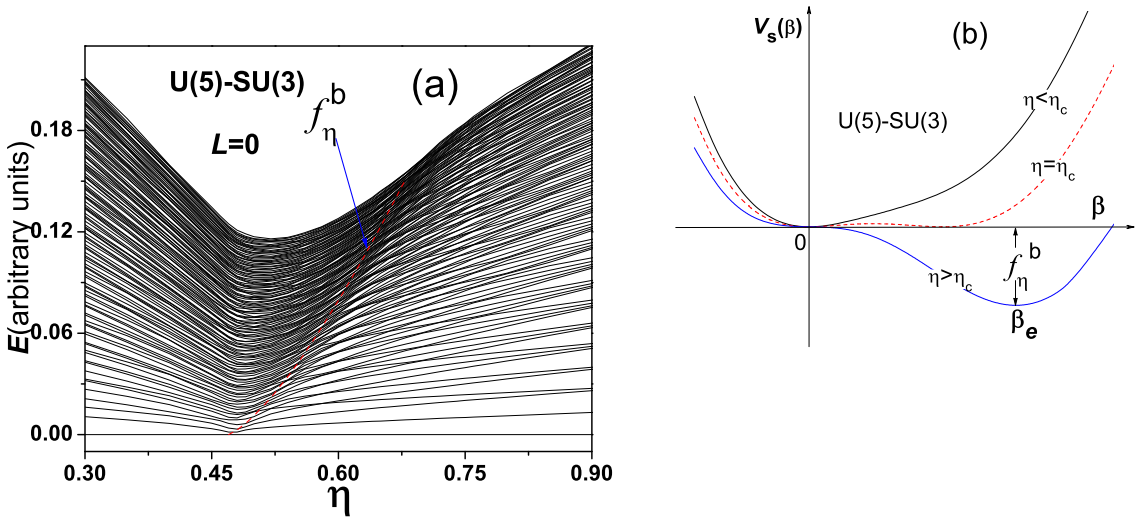

FIG. 6: (Color online) The same as in Fig. 3 but for the low-lying $L=0$ spectrum obtained from the U(5)-SU(3) Hamiltonian from (1) with $N=100$ and $\chi=-\frac{\sqrt{7}}{2}$, as well as the typical potential structure in the transitional region derived from (3) with $\chi=-\frac{\sqrt{7}}{2}$.

As a comparison, the behaviors of $\rho(E)$ with $L=0$ as functions of the excitation energy in the U(5), the SO(6), and the SU(3) limits are shown in Fig. 5. One can find from Fig. 5(a) that $\rho(E)$ in the U(5) limit shows a linear increment, which is similar to the behavior of the dashed line shown in Fig. 4(c). In contrast, the results in Fig. 5(b) show that $\rho(E)$ in the SO(6) limit presents a fluctuating behavior, which is similar to that given in Fig. 4(a). It further confirms that the ESQPT shown in Fig. 4 is just the transition from the SO(6)-like spectrum to the U(5)-like spectrum. Notably, the fluctuational behavior of $\rho(E)$ in the U(5)-like spectrum as shown in Fig. 4(c) is completely different from that in the SO(6) limit. In addition, the results shown in Fig. 5(c) indicate that $\rho(E)$ in the SU(3) limit may present another fluctuating behavior different from that in the SO(6) limit. Although the feature of $\rho(E)$ in each limit will be more or less altered by adding some terms with different symmetry perturbatively, the qualitative characteristic of $\rho(E)$ is solely determined by the dominant symmetry in the IBM. Therefore, in principle, the type of the spectrum and the corresponding ESQPT can be recognized from the behavior of $\rho(E)$.

B. the U(5)-SU(3) ESQPT

Unlike the U(5)-SO(6) case, the U(5)-SU(3) GSQPT is proven to be the first-order transition [1]. To check the spectral characteristics in this transitional region, the lowest 124 levels with $L=0$ as functions of the control parameter η obtained from the U(5)-SU(3) transitional Hamiltonian from (1) with $\chi=-\sqrt{7}/2$ and $N=100$ are show in Fig. 6(a). Similarly, we can define the separatrix function in the U(5)-SU(3) transitional region as the difference between the value of the energy function (3) with $\chi=-\sqrt{7}/2$ evaluated at $\beta=0$ and that at β_e. It is formally given as

$$f_\eta^b=\begin{cases} 0, & 0\le\eta\le\eta_c, \\ \frac{\tilde\beta^2(16\eta+9\eta\tilde\beta^2+4\sqrt{2}\eta\tilde\beta-8\tilde\beta^2-8)}{8(1+\tilde\beta^2)^2}, & \eta_c<\eta\le 1, \end{cases} \tag{7}$$

with $\tilde\beta$ being determined by the equation

$$\eta=\frac{4\tilde\beta^2+4}{\tilde\beta^2+3\sqrt{2}\tilde\beta+8-\sqrt{2}\tilde\beta^3}. \tag{8}$$

The definition of f_η^b is also illustrated in the right panel of Fig. 6, in which the potential evolution in the U(5)-SU(3) transitional region is clearly shown. It can be observed from the left panel of Fig. 6 that the spectrum in the U(5)-SU(3) transitional region can be clearly divided into two sets by the separatrix f_η^b, which starts from the ground state energy at the critical point $\eta=\eta_c$ to the top of the spectrum at $\eta>\eta_c$ (even at $\eta=1$ if all the 884 $L=0$ excited levels for $N=100$ are taken into account). Specifically, the energy levels above the separatrix show relatively high local level densities, while those below the separatrix present a lot of level crossing and relatively low local level densities. It is thus expected that a new type of ESQPT may occur around the separatrix with the increasing of the excitation energy. Similar to the U(5)-SO(6) ESQPT, the potential evolution shown in the right panel of Fig. 6 indicates that this new type of ESQPT may appear only when $\eta>\eta_c$ [14].

To further reveal the potential ESQPT, the effective order parameter $\rho(E)$ is also applied to indicate the ESQPT signal in this transitional region. Similarly, $\rho(E)$ curves as functions of the excitation energy for three typical η values are provided in Fig. 7. One can observe from panels (a) and (c) that the fluctuational behavior of $\rho(E)$ of the SU(3)-like spectrum ($\eta=0.9$) and that of the U(5)-like spectrum ($\eta=0.4$) are completely different, which are highlighted by

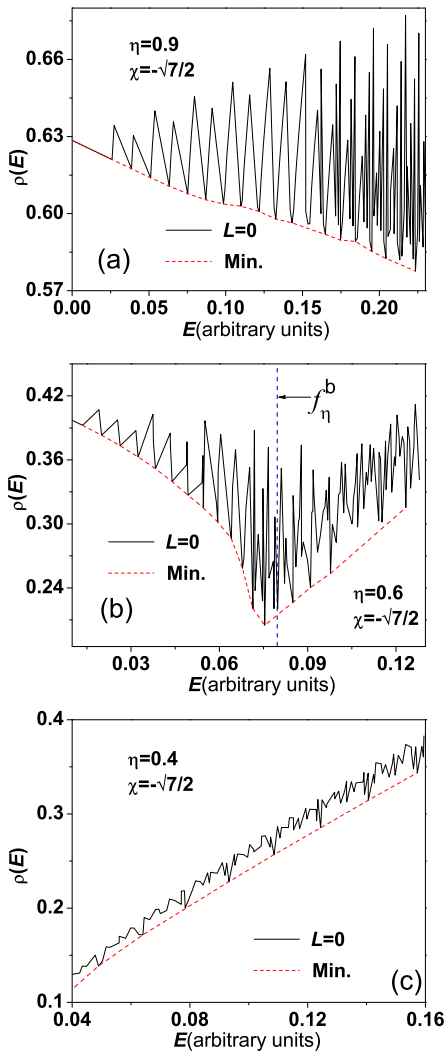

FIG. 7: (Color online) (a) $\rho(E)$ for $L=0$ obtained from the U(5)-SU(3) Hamiltonian with $N=100$ and $\eta=0.9$ as a function of the excitation energy, where the dashed line denotes the local minima of $\rho(E)$. (b) The same as in (a) but for the results at $\eta=0.6$. (c) The same as in (a) but for the results at $\eta=0.4$.

the dashed lines connecting the local minima of $\rho(E)$ in the two cases. Specifically, the dashed line in the SU(3)-like spectrum presents a monotonic decrement but that in the U(5)-like spectrum shows a monotonic increment, which is actually consistent in the main characteristic of $\rho(E)$ in the corresponding limiting cases shown in Fig. 5. It is more interesting to see from Fig. 7(b) that the fluctuational behavior of $\rho(E)$ at $\eta=0.6$ displays the combined features of that shown in Fig. 7(a) and Fig. 7(c), and shows a transition around the separatrix point with $E=0.075$. The phenomenon is quite similar to that occurring in the U(5)-SO(6) case shown in Fig. 4. One can thus conclude that the ESQPT indeed occurs in the U(5)-SU(3) transitional region (the U(5)-SU(3) ESQPT). Meanwhile, the results also justify the validity of the effective order parameter $\rho(E)$ in the U(5)-SU(3) ESQPT. It should be noted that one may find exactly the same spectral feature in the U(5)-$\overline{\text{SU(3)}}$ transitional region just by replacing χ with $-\chi$.

On the other hand, it has been revealed that there exists a chaotic region within the U(5)-SU(3) transitional region [30–33], where the spectral statistics with a fixed angular momentum such as $L=0$ indicate strong chaos [33]. The range of the chaotic region may lie between the critical point and the SU(3) limit, where the U(5)-SU(3) ESQPT also occurs as shown in Fig. 6. Therefore, the spectrum at a ESQPT point in the U(5)-SU(3) region, such as that at $\eta=0.6$ shown in Fig. 6, may contain both U(5)-like levels and SU(3)-like levels. Thus, one may conclude that the chaotic behavior of the spectrum in the U(5)-SU(3) transitional region might be due to the spectrum involving these two different types of excited states simultaneously. Although the similar situation may also occur in the U(5)-SO(6) ESQPT region, the level statistics in the whole U(5)-SO(6) region is always regular just due to the common SO(5) sub-symmetry [30–32].

D. the SU(3)-SO(6) ESQPT

Based on the Hamiltonian (1) with $\eta=1$, it can be proven that the SO(6) limit may exactly coincide with the critical point of the SU(3)-$\overline{\text{SU(3)}}$ GSQPT [34], but there is no GSQPT in the SU(3)-SO(6) transitional region corresponding to $\chi\in[-\sqrt{7}/2,\ 0]$ or $\overline{\text{SU(3)}}$-SO(6) transitional region corresponding to $\chi\in[0,\ \sqrt{7}/2]$ [1]. However, it has been known for many years that there exists a chaotic region in the SU(3)-SO(6) transitional region [30, 31, 33, 35], which in turn suggests that there may exist the SU(3)-SO(6) ESQPTs occurring in this transitional region according to the previous analysis. In order to verify the ESQPTs, the lowest 124 levels with $L=0$ as functions of the control parameter χ obtained from (1) with $\eta=1$ are shown in Fig. 8, in which the potential evolution in this transitional region is also shown. Similarly, one can define a separatrix function f^c_χ in the SU(3)-SO(6) transitional region as the difference between the value of the energy function (3) with $\eta=1$ evaluated at the global minimum (β_e) and that at the local minimum, which is given as

$$f^c_\chi=\frac{-\chi\sqrt{14+\chi^2}}{14},\qquad -\frac{\sqrt{7}}{2}\le\chi\le 0. \tag{9}$$

It is clear that the spectral pattern in the SU(3)-$\overline{\text{SU(3)}}$ transitional region with $\chi\in[-\sqrt{7}/2,\sqrt{7}/2]$ are exactly symmetric by changing χ to $-\chi$ [29, 34] as shown in the left panel of Fig. 8. More importantly, there indeed exists noticeable change in the level density along the separatrix starting from the ground state energy in the SO(6) limit to the top of the spectrum, which just indicates the occurrence of the ESQPT in the SU(3)-SO(6) region. The same level density change also occurs in the $\overline{\text{SU(3)}}$-SO(6) transitional region corresponding to $\chi\in[0,\ \frac{\sqrt{7}}{2}]$, in which the separatrix $f^c_{-\chi}$ shown in Fig. 8 can be derived from (9) by changing χ to $-\chi$. In addition, the potential evolution shown in the right panel of Fig. 8 indicates that the ESQPTs should begin from the SO(6) limit corresponding to $f^c_\chi=f^c_{-\chi}=0$.

To figure out the type of the ESQPT in the SU(3)-SO(6) transitional region, $\rho(E)$ curves as functions of the excitation

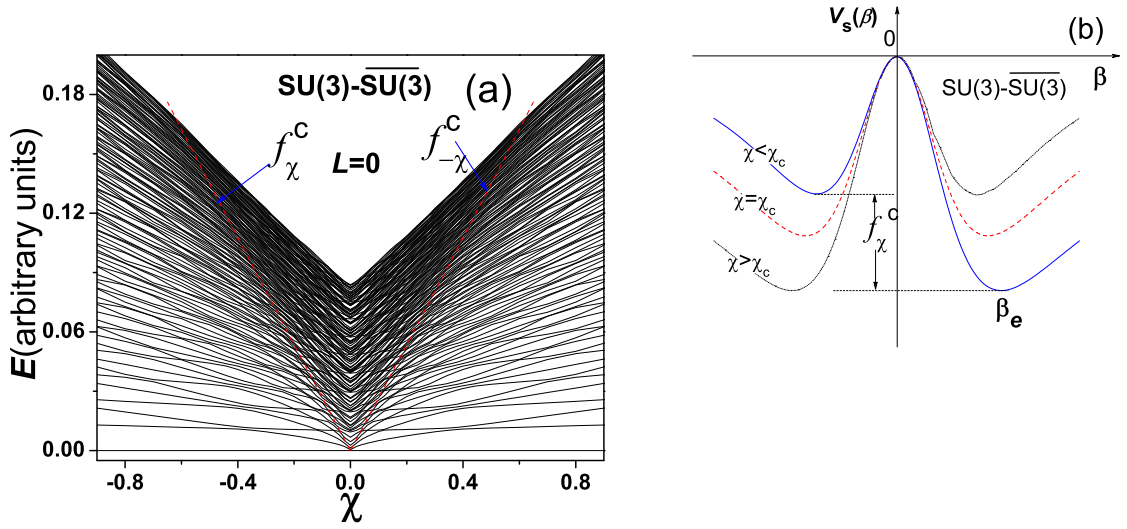

FIG. 8: (Color online) The same as in Fig. 3 but for the low-lying $L = 0$ spectrum obtained from the SU(3)-$\overline{\text{SU(3)}}$ Hamiltonian obtained from (1) with $\eta = 1$ and $N = 100$, as well as the typical potential structure in this transitional region derived from (3) with $\eta = 1$.

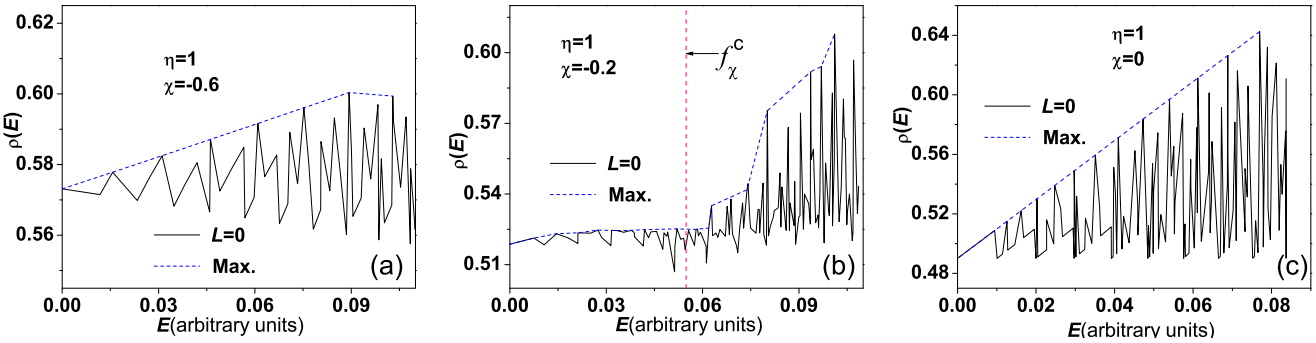

FIG. 9: (Color online) (a) $\rho(E)$ for $L = 0$ as a function of the excitation energy obtained from the SU(3)-$\overline{\text{SU(3)}}$ Hamiltonian with $N = 100$ at $\chi = -0.6$, where the dashed line denotes the local maxima of $\rho(E)$. (b) The same as in (a) but for the results at $\chi = -0.2$. (c) The same as in (a) but for the results at $\chi = 0$.

energy for three typical χ values are calculated, of which the results are shown in Fig. 9. One can observe from Fig. 9(a) and Fig. 9(c) that, in both the SU(3)-like spectrum ($\chi = -0.6$) and the SO(6) spectrum ($\chi = 0$), $\rho(E)$ fluctuates with the variation of E, but the main feature of the fluctuating behavior in the two cases are completely different, which is highlighted by the dashed lines connecting the local maxima of $\rho(E)$. Specifically, the dashed line in the SU(3)-like spectrum shows a slight increasing, but it in the SO(6) spectrum increases with the increasing of E significantly. The fluctuation amplitude of $\rho(E)$ in this case becomes much larger than that in the SU(3)-like case within the same energy range, which actually agrees with the results shown in Fig. 5. Hence, one can conclude from Fig. 9(b) that the sudden increasing in the fluctuation amplitude of $\rho(E)$ around the separatrix point $E = 0.054$ is just a signature of the SU(3)-SO(6) ESQPT. The same conclusion can apply to the $\overline{\text{SU(3)}}$-SO(6) ESQPT since $\rho(E)$ is symmetric with respect to the replacement of χ with $-\chi$. In addition, the results in Fig. 9(b) also indicate that the separatrix defined in the large-N limit may not exactly coincide with the real separatrix point of the ESQPT in finite-N cases due to the finite-N effect [14].

E. the SU(3)-SO(6)-U(5) ESQPT

We have shown the ESQPTs appearing on the three legs of the extended Casten triangle shown in Fig. 1. For the situations inside the extended Casten triangle, we take the case with $\eta = 0.8$ to illustrate the possible ESQPTs in the transitional region along the χ axis and the case with $\chi = -0.5$ to illustrate the ESQPTs in the transitional region along the η axis.

Firstly, in order to observe the spectral distribution globally, 500 low-lying levels with $L = 0$ as functions of the control parameter χ obtained from (1) with $\eta = 0.8$, together with the corresponding potential evolution, are shown in Fig. 10. For a given potential surface, we can define two separatrix func-

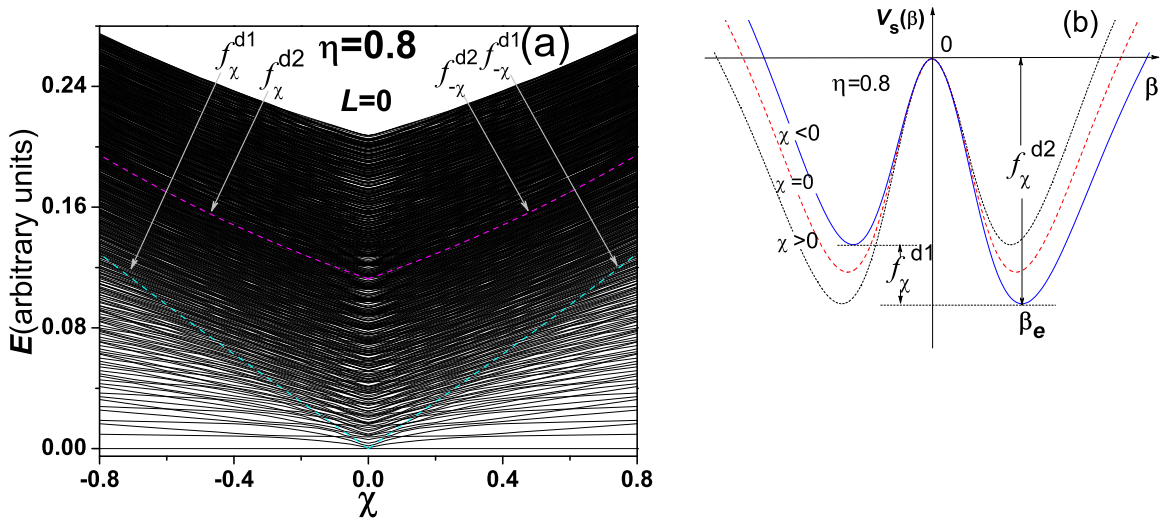

FIG. 10: (Color online) The spectrum of 500 low-lying levels with $L = 0$ obtained from the Hamiltonian (1) with $\eta = 0.8$ and $N = 100$, and the typical potential structures in this case.

tions as shown in Fig. 10(b), in which f_χ^{d1} is the difference between its global minimum evaluated at $\beta = \beta_e$ and its local minimum, while f_χ^{d2} is the difference between its global minimum evaluated at $\beta = \beta_e$ and its local maximum evaluated at $\beta = 0$. Specifically, the two separatrix functions at $\eta = 0.8$ as functions of χ with $\chi \in [-\frac{\sqrt{7}}{2}, 0]$ are given as

$$f_\chi^{d1} = \frac{\tilde{\beta}_a^3(-\tilde{\beta}_a + \sqrt{4+\frac{3}{\tilde{\beta}_a^2}+\tilde{\beta}_a^2})}{10(1+\tilde{\beta}_a^2)} + \frac{\tilde{\beta}_b^3(\tilde{\beta}_b + \sqrt{4+\frac{3}{\tilde{\beta}_b^2}+\tilde{\beta}_b^2})}{10(1+\tilde{\beta}_b^2)} \quad (10)$$

and

$$f_\chi^{d2} = \frac{\tilde{\beta}_b^3(\tilde{\beta}_b + \sqrt{4+\frac{3}{\tilde{\beta}_b^2}+\tilde{\beta}_b^2})}{10(1+\tilde{\beta}_b^2)} \quad (11)$$

with $\tilde{\beta}_a$ and $\tilde{\beta}_b$ being the negative and positive solution of the equation

$$\chi = \frac{3\sqrt{14}-\sqrt{14}\tilde{\beta}^2}{4\tilde{\beta}} - \frac{\sqrt{14}}{4}\sqrt{\frac{3}{\tilde{\beta}^2}+\tilde{\beta}^2+4}. \quad (12)$$

It should be mentioned that the two different separatrix functions coexisting in an ESQPT was also observed from the anharmonicity effect [16] in the U(2)-SU(3) ESQPT in the VM by introducing the second-order Casimir operator of the U(2). As shown in Fig. 10(a), the $L = 0$ spectrum for a given χ can be divided by the two separatrix lines into three sets when $\chi \neq 0$ or two sets when $\chi = 0$. It is thus expected that there may be the ESQPT occurring across three different spectral patterns when $\chi \neq 0$. In addition, it is obvious that the whole spectrum within $\chi \in [-\sqrt{7}/2, \sqrt{7}/2]$ is exactly symmetric with respect to $\chi = 0$ axis as shown in Fig. 10. Thus, the separatrix functions are also symmetric with respect to $\chi = 0$ axis.

To identify the type of the possible ESQPT, $\rho(E)$ curves for two typical χ values as functions of the excitation energy are calculated, which are shown in Fig. 11. In addition, the spectrum corresponding to that shown in Fig. 10 with $-0.6 \leq \chi \leq -0.4$ is also shown on an expanded scale in Fig. 11 in order to have a better view of how the spectrum is divided by the two separatrix lines. As shown in Fig. 11(a), the level pattern above each separatrix line is quite different from that below the separatrix line, which hints that the ESQPTs may occur around the separatrix. And indeed, the effective order parameter $\rho(E)$ shown in Fig. 11(b) further confirms the emergence of the ESQPTs. Specifically, the results show that the level pattern at $\chi = -0.5$ may transform from the SU(3)-like one (with small fluctuations in $\rho(E)$) to the SO(6)-like one (with relatively large fluctuations in $\rho(E)$) around the first separatrix point $E = 0.08$; with the increasing of E, the level pattern may transform to the U(5)-like one around the second separatrix point $E = 0.16$. The two ESQPTs can be highlighted by the dashed lines connecting either the local maxima or the local minima of $\rho(E)$. These two ESQPTs are denoted together as the SU(3)-SO(6)-U(5) ESQPT. The SU(3)-SO(6)-U(5) ESQPT may generally appear when $\chi < 0$ as shown in Fig. 10(a). By replacing χ with $-\chi$, one can deduce that the $\overline{\text{SU(3)}}$-SO(6)-U(5) ESQPT may generally occur when $\chi > 0$. When $\chi = 0$, one can observe from Fig. 11(c) that the U(5)-SO(6) ESQPT may occur around the separatrix point $E = 0.11$, which actually agrees with the corresponding case shown in Fig. 2.

To reveal the possible ESQPTs appearing in the transitional region inside the extended Casten triangle along the η axis, 300 low-lying levels with $L = 0$ as functions of the control

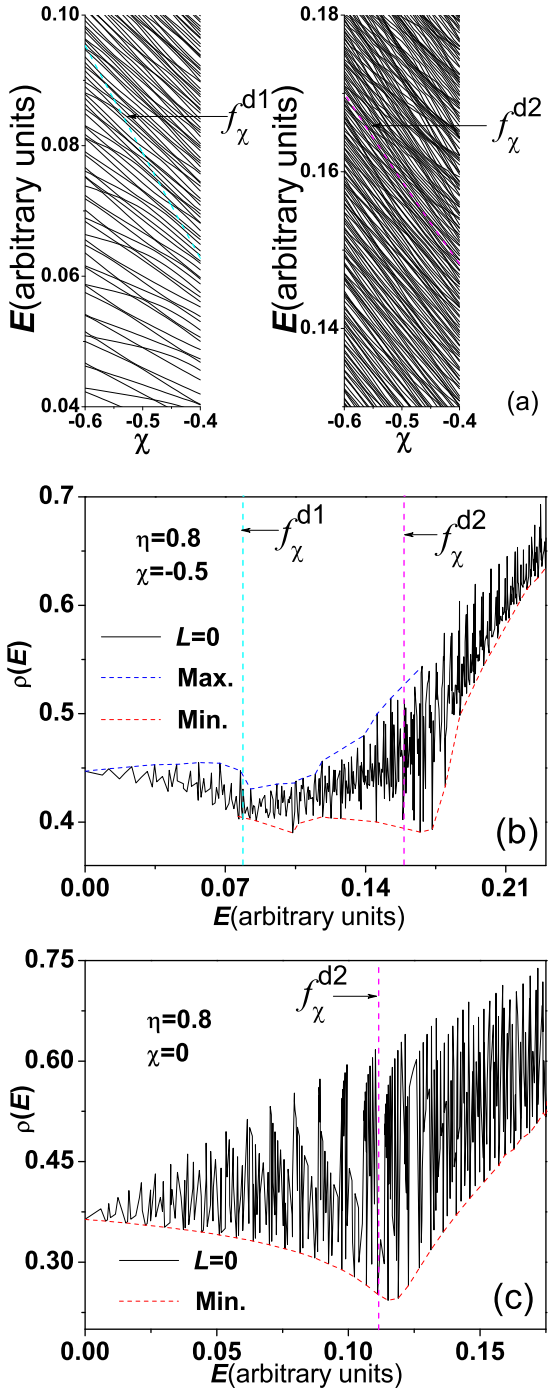

FIG. 11: (Color online) (a) The spectral pattern on an expanded scale corresponding to the spectrum shown in Fig. 10 within $\chi \in [-0.6, -0.4]$. (b) $\rho(E)$ at $(\eta, \chi) = (0.8, -0,5)$ as a function of the excitation energy, where the local maxima and minima are connected by the dashed lines. (c) The same as in (b) but for $\rho(E)$ at $(\eta, \chi) = (0.8, 0)$.

parameter η obtained from (1) with $\chi = -0.5$, together with the corresponding potential evolution, are shown in Fig. 12. As shown in Fig. 12(a), the levels can also be divided into three sets by the two separatrix lines for relatively larger η values, with which the spectral pattern, especially its density, in different set seems also different. The results indicate that there may exist the ESQPTs occurring along the two separatrix lines. The corresponding potential evolution shown in Fig. 12(b) further indicates that the ESQPT in this case may only appear when $\eta > \eta_c$. Similarly, the two separatrix functions in this case can be defined according to the corresponding potential structure shown in Fig. 12(b), which are formally given as

$$f_\eta^{e1} = \frac{\tilde{\beta}_c^3(-2\sqrt{14}+55\tilde{\beta}_c+2\sqrt{14}\tilde{\beta}_c^2)}{2(1+\tilde{\beta}_c^2)(-56-3\sqrt{14}\tilde{\beta}_c-\tilde{\beta}_c^2+\sqrt{14}\tilde{\beta}_c^3)} - \frac{\tilde{\beta}_d^3(-2\sqrt{14}+55\tilde{\beta}_d+2\sqrt{14}\tilde{\beta}_d^2)}{2(1+\tilde{\beta}_d^2)(-56-3\sqrt{14}\tilde{\beta}_d-\tilde{\beta}_d^2+\sqrt{14}\tilde{\beta}_d^3)} \quad (13)$$

and

$$f_\eta^{e2} = \frac{\tilde{\beta}_d^3(-2\sqrt{14}+55\tilde{\beta}_d+2\sqrt{14}\tilde{\beta}_d^2)}{2(1+\tilde{\beta}_d^2)(-56-3\sqrt{14}\tilde{\beta}_d-\tilde{\beta}_d^2+\sqrt{14}\tilde{\beta}_d^3)} \quad (14)$$

with $\tilde{\beta}_c$ and $\tilde{\beta}_d$ representing the negative and positive solution of the equation

$$\eta = \frac{28+28\tilde{\beta}^2}{56+3\sqrt{14}\tilde{\beta}+\tilde{\beta}^2-\sqrt{14}\tilde{\beta}^3}. \quad (15)$$

To figure out the type of these ESQPTs, the $\rho(E)$ curves for three typical η values as functions of the excitation energy are shown in Fig. 13. As shown in Fig. 13(a), the behavior of $\rho(E)$ indicates that there is an SU(3)-SO(6) ESQPT occurring in the spectrum at $(\chi,\ \eta) = (-0.5,\ 0.9)$ around $E = 0.11$. The results shown in Fig. 13(b) indicate that the SU(3)-SO(6)-U(5) ESQPT may occur in the spectrum at $(\chi,\ \eta) = (-0.5,\ 0.7)$. One can thus conclude that the ESQPT in the spectrum shown in Fig. 12(a) is either of the SU(3)-SO(6)-U(5) type or of the SU(3)-SO(6) type. When $\eta < \eta_c$, the example shown in Fig. 13(c) shows that there is no ESQPT occurring in this case. In addition, the results also justify that $\rho(E)$ is still qualified to be taken as the effective order parameter inside the extended Casten triangle.

From the mean-field perspective, the spectral pattern here referred to as the U(5)-like, the SO(6)-like, or the SU(3)-like means that the levels are confined within the corresponding potential. For example, the SO(6)-like spectrum shown in Fig. 12 refers to those with $f_\chi^{e2} > E > f_\chi^{e1}$, while the corresponding potential indicates that this type of spectrum may be affected by the prolate and the oblate minimum simultaneously just as that in the SO(6) limit. Most importantly, the results shown in Fig. 13 indicate that the behavior of $\rho(E)$ within the SO(6)-like spectral pattern is indeed more like that in the SO(6) limit in comparison to that in the U(5) or the SU(3) limit. Similar argument also apply to the U(5)-like and SU(3)-like spectra.

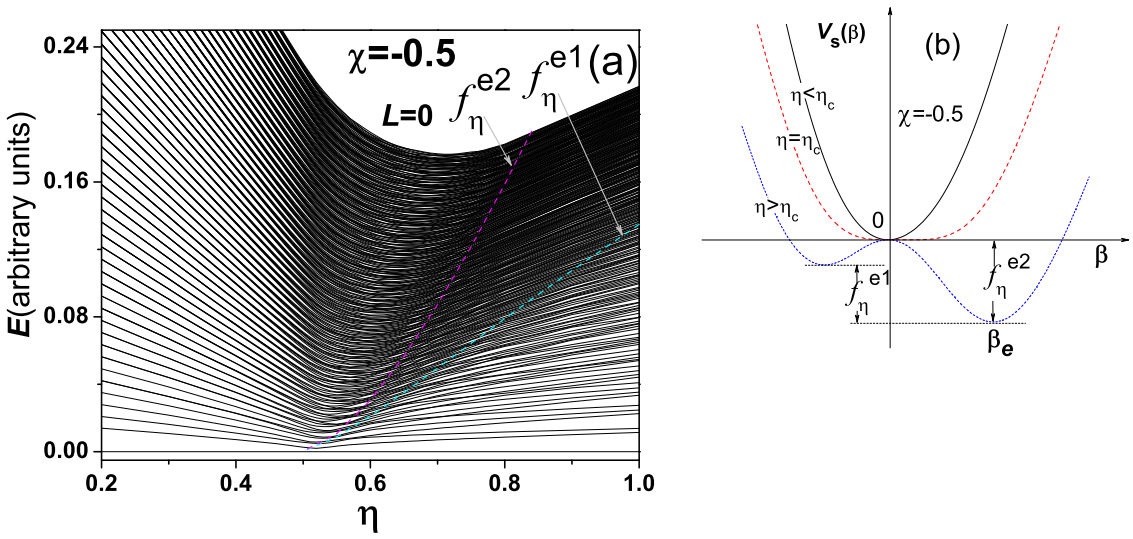

FIG. 12: (Color online) The same as in Fig. 10 but for the low-lying $L = 0$ spectrum obtained from the Hamiltonian (1) with $\chi = -0.5$ and $N = 100$, and the typical potential structures in this case.

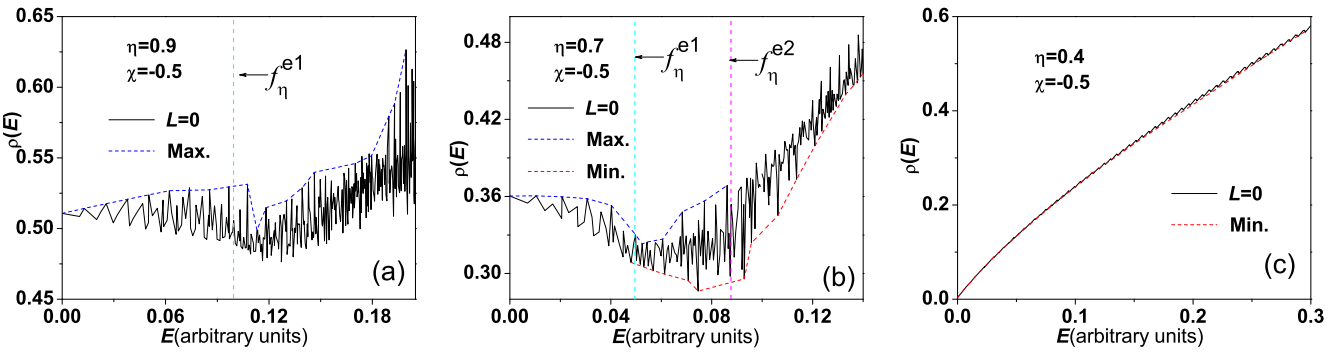

FIG. 13: (Color online) (a) $\rho(E)$ at $(\eta,\chi) = (0.9,-0,5)$ as a function of the excitation energy, where the local maxima of $\rho(E)$ are connected by the dashed line. (b) The same as in (a) but for the results at $(\eta,\chi) = (0.7,-0.5)$. (c) The same as in (a) but for the results at $(\eta,\chi) = (0.4,-0.5)$, where the local minima of $\rho(E)$ are connected by the dashed line.

IV. POSSIBLE EXTENSION OF THE PHASE DIAGRAM

Base on the discussions in Sec. III, it can be realized that the ESQPTs in the IBM are much more abundant than previously recognized. The concept of phase for a given quantum system, such as the shape phases of atomic nuclei, is traditionally defined only for the ground state [1], but the properties of the lowest-lying states are indeed heavily affected by the ground state, which indicate that a specific phase can be also applied for the lowest-lying states [14]. However, the emergence of the ESQPTs identified in this work indicates that the properties of excited states may evidently change around the separatrix point with the increasing of the excitation energy. If the afore mentioned U(5)-like, SO(6)-like, and SU(3)-like (or $\overline{\text{SU(3)}}$-like) excited states are roughly attributed to three different dynamical phases, one can further extend the IBM phase diagram as shown in Fig. 1 with the axis of the excitation energy, which is schematically illustrated in Fig. 14. As illustrated in Fig. 14, the possible new phase diagram is three-dimensional with the bottom area being the original ground-sate phase diagram shown in Fig. 1. The phase boundary corresponding to (1) should be principally determined in the large-N limit by the potential energy surface given in (3).

As mentioned previously, ESQPT may also occur with variation of the control parameters in the Hamiltonian [14]. To further explore the phase diagram indicated in Fig. 14, we choose the case with $\eta = 0.8$ and the case with $\chi = -0.5$ as examples to illustrate the ESQPTs occurring with variation of χ or η. Notably, the level patterns and the corresponding potential structure in these two cases can be found in Fig. 10 and Fig. 12. Several typical 0^+ levels and the effective order parameter ρ as functions of χ or η are shown in Fig. 15. As shown in Fig. 15(a), the energy levels of the 0^+_{28} and 0^+_{39} states in the $\eta = 0.8$ case evolve from the SU(3)-like to the SO(6)-like, and then to the $\overline{\text{SU(3)}}$-like with the increasing of

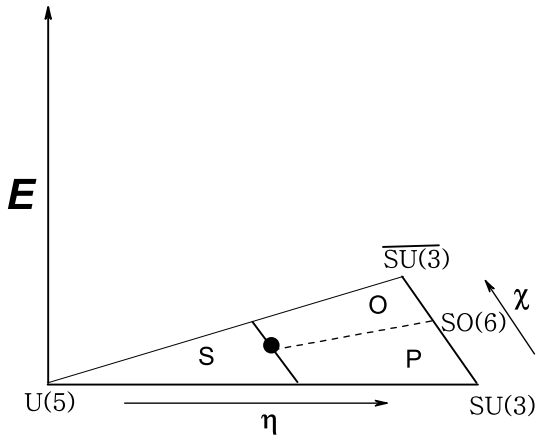

FIG. 14: (Color online) The schematic phase diagram of the IBM extended towards the excitation energy.

χ from negative to positive, which thus indicates an SU(3)-SO(6)-$\overline{\text{SU(3)}}$ ESQPT. In contrast, the 0_1^+ ground state level may evolve directly from the SU(3)-like to the $\overline{\text{SU(3)}}$-like, which just reflects the SU(3)-$\overline{\text{SU(3)}}$ GSQPT. Moreover, the results shown in Fig. 15(b) indicate that the fluctuation behavior of $\rho(\chi)$ for the excited states in the SO(6)-like region are clearly different from that in the SU(3)-like or the $\overline{\text{SU(3)}}$-like region, which further confirms the occurrence of the SU(3)-SO(6)-$\overline{\text{SU(3)}}$ ESQPT, while the linear behavior of $\rho(\chi)$ for the ground state justifies the SU(3)-$\overline{\text{SU(3)}}$ GSQPT. As further shown in Fig. 15(c), the 0_{31}^+ and 0_{51}^+ levels in the $\chi = -0.5$ case may evolve from the U(5)-like to the SO(6)-like, and then to the SU(3)-like, which indicates a U(5)-SO(6)-SU(3) ESQPT occurring in this case. The behavior of $\rho(\eta)$ shown in Fig. 15(d) further confirms the occurrence of the U(5)-SO(6)-SU(3) ESQPT, as well as the U(5)-SU(3) GSQPT. Here, the ESQPT is classified according to the order of the spectral pattern appearing with the increasing of the control parameter η or χ. Anyway, it seems that the effective order parameter ρ is still valid to identify the ESQPT with variation of the control parameters.

As we know, the GSQPTs in the IBM have been experimentally confirmed in nuclei [5] because the main features of the phase transitions persist even for moderate $N \sim 10$ as analyzed by Iachello and Zamfir [28]. It would be interesting to check whether the main features of the ESQPTs can even survive for $N \sim 10$, which is, however, not the topic of this work. In addition, the finite-N effects may also provide a certain correction on the phase diagram.

V. SUMMARY

In summary, the ESQPTs in the IBM have been systematically investigated through analyzing the characteristics of the $L = 0$ excited states. Specifically, it was confirmed that the U(5)-SO(6) ESQPT previously recognized in the $\tau = 0$ spectra may emerge even in the $L = 0$ spectra, which thus provides a paradigm to discuss the possible ESQPTs in other transitional regions in the IBM. It is further observed that the similar ESQPTs may emerge in the U(5)-SU(3) transitional region, the SU(3)-$\overline{\text{SU(3)}}$ transitional region, and even inside the Extended Casten triangle. Particularly, the ESQPTs in some cases, such as those shown in Fig. 10 and Fig. 12, may cross three phases with different spectral patterns. The ESQPTs in the IBM have been further justified by the evolutional behavior of the effective order parameter ρ. In turn, the results suggest that the IBM can provide a very convenient theoretical framework to examine different types of ESQPT as it dose for the GSQPT. In addition, the relation between the ESQPT and the chaotic dynamics in the IBM has been stated, and a possible extension of the IBM phase diagram toward the excitation energy has been also discussed briefly.

Currently, the most promising physical systems for finding experimental evidences of ESQPTs are molecules [14, 16, 36–38]. Nevertheless, our analysis indicates that the IBM involves much richer ESQPTs than previously recognized, which may in turn offer some chances to search for ESQPTs in nuclei. However, more detailed investigation is still needed. Related work is in progress.

Acknowledgments

Support from U.S. National Science Foundation (OCI-0904874), Southeastern Universities Research Association, the Natural Science Foundation of China (11375005, 11005056, and 11375080), and the LSU–LNNU joint research program (9961) is acknowledged.

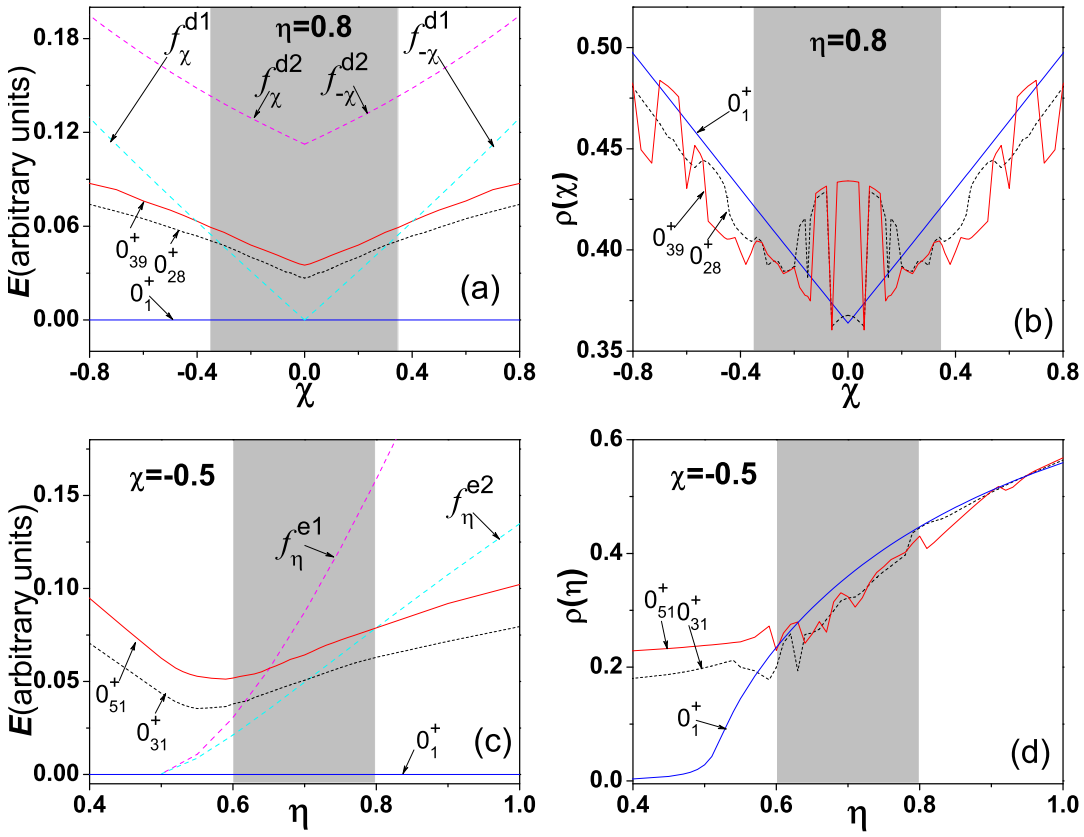

FIG. 15: (Color online) (a) Three typical 0^+ energy levels as functions of the control parameter χ obtained from the Hamiltonian (1) with $\eta = 0.8$ and $N = 100$. (b) The effective order parameter ρ corresponding to (a) as a function of χ. (c) Three typical 0^+ energy levels as functions of the control parameter η obtained from the Hamiltonian (1) with $\chi = -0.5$ and $N = 100$. (d) The effective order parameter ρ corresponding to (c) as a function of η.

[1] F. Iachello, and A. Arima, *The Interacting Boson Model* (Cambridge University, Cambridge, England, 1987).
[2] F. Iachello, and R. D. Levine, *Algebraic Theory of Molecules* (Oxford University, Oxford, UK 1995).
[3] R. F. Casten and E. A. McCutchan, J. Phys. G **34**, R285 (2007).
[4] P. Cejnar, and J. Jolie, Prog. Part. Nucl. Phys. **62**, 210 (2009).
[5] P. Cejnar, J. Jolie, and R. F. Casten, Rev. Mod. Phys. **82**, 2155 (2010).
[6] W. D. Heiss and M. Müller, Phys. Rev. E **66**, 016217 (2002).
[7] W. D. Heiss, F. G. Scholtz and H. B. Geyer, J. Phys. A **38**, 1843 (2005).
[8] F. Leyvraz and W. D. Heiss, Phys. Rev. Lett. **95**, 050402 (2005).
[9] S. Heinze, P. Cejnar, J. Jolie, and M. Macek, Phys. Rev. C **73**, 014306 (2006).
[10] M. Macek, P. Cejnar, J. Jolie, and S. Heinze, Phys. Rev. C **73**, 014307 (2006).
[11] P. Cejnar, M. Macek, S. Heinze, J. Jolie, and J. Dobeš, J. Phys. A **39**, L515 (2006).
[12] M. Macek, P. Stránský, P. Cejnar, S. Heinze, J. Jolie, and J. Dobeš, Phys. Rev. C **75**, 064318 (2007).
[13] P. Cejnar and P. Stránský, Phys. Rev. E **78**, 031130 (2008).
[14] M. A. Caprio, P. Cejnar, and F. Iachello, Ann. Phys. **323**, 1106 (2008).
[15] F. Pérez-Bernal and F. Iachello, Phys. Rev. A **77**, 032115 (2008).
[16] F. Pérez-Bernal and O. Álvarez-Bajo, Phys. Rev. A **81**, 050101(R) (2010).
[17] L. F. Santos and F. Pérez-Bernal, Phys. Rev. A **92**, 050101(R) (2015).
[18] P. Stránský, M. Macek, and P. Cejnar, Ann. Phys. **345**, 73 (2014).
[19] P. Stránský, M. Macek, A. Leviatan, and P. Cejnar, Ann. Phys. **356**, 57 (2015).
[20] P. Pérez-Fernández, A. Relaño, J. M. Arias, J. Dukelsky, and J. E. García-Ramos, Phys. Rev. A **80**, 032111 (2009).
[21] Z.-G. Yuan, P. Zhang, S.-S. Li, J. Jing, and L.-B. Kong, Phys. Rev. A **85**, 044102 (2012).
[22] P. Pérez-Fernández, P. Cejnar, J. M. Arias, J. Dukelsky, J. E. García-Ramos, and A. Relaño, Phys. Rev. A **83**, 033802 (2011).
[23] P. Pérez-Fernández, A. Relaño, J. M. Arias, P. Cejnar, J. Dukelsky, and J. E. García-Ramos, Phys. Rev. E **83**, 046208 (2011).
[24] T. Brandes, Phys. Rev. E **88**, 032133 (2013).
[25] V. M. Bastidas, P. Pérez-Fernández, M. Vogl, and T. Brandes, Phys. Rev. Lett **112**, 140408 (2014).
[26] R. J. Casperson, Commput. Phys. Comm. **183**, 1029 (2012).
[27] D. D. Warner and R. F. Casten, Phys. Rev. C **28**, 1798 (1983).
[28] F. Iachello and N. V. Zamfir, Phys. Rev. Lett. **92**, 212501 (2004).
[29] J. Jolie, P. Cejnar, R. F. Casten, S. Heinze, A. Linnemann, and V. Werner, Phys. Rev. Lett. **89**, 182502 (2002).
[30] Y. Alhassid and N. Whelan, Phys. Rev. Lett. **67**, 816 (1991).
[31] N. Whelan and Y. Alhassid, Nucl. Phys. A **556**, 42 (1993).
[32] P. Cejnar and J. Jolie, Phys. Rev. E **58**, 387 (1998).
[33] S. Karampagia, D. Bonatsos, and R. F. Casten, Phys. Rev. C **91**, 054325 (2015).
[34] J. Jolie, R. F. Casten, P. von Brentano, and V. Werner, Phys. Rev. Lett. **87**, 162501 (2001).
[35] Y. Alhassid, A. Novoselsky, N. Whelan, Phys. Rev. Lett. **65**, 2971 (1990).
[36] D. Larese and F. Iachello, J. Mol. Struct. **1006**, 611 (2011).
[37] D. Larese, F. Pérez-Bernal, and F. Iachello, J. Mol. Struct. **1051**, 310 (2013).
[38] D. Larese, M. A. Caprio, F. Pérez-Bernal, and F. Iachello, J. Chem. Phys. **140**, 014304 (2014).